ONE-DIMENSIONAL THEORY OF THE WAVE BOUNDARY LAYER

D. V. CHALIKOV[1] and M. Yu. BELEVICH[2]

[1]*National Meteorological Center, World Wea. Bldg. W/NMC 2 5200 Auth Road, Washington, D.C., 20233, U.S.A.* [2]*St. Petersburg Branch, Institute of Oceanology Russian Acad. Sci. 30, Pervaya Liniya, 199053, St. Petersburg, Russia*

(Received in final form 2 June, 1992)

Abstract. Results obtained in a 2-D modeling of the statistical structure of the wave boundary layer (WBL) are used for elaboration of the general approach to 1-D modeling taking into account the spectral properties of wave drag for an arbitrary wave field. In the case of the wave field described by the JONSWAP spectrum, the momentum and energy spectral density exchange, vertical profiles of the wave-induced momentum flux and dependence of total roughness parameter and drag coefficient on peak frequency are given. The reasons that the total roughness parameter increases with decreasing fetch are explained. The role of wind waves as an active element of the ocean-atmosphere dynamic system is also discussed.

1. Introduction

The structure of the atmospheric boundary layer above the sea for neutral density stratification is as a whole rather close to the self-similar one. However, near the surface the role of wave-induced fluctuations increases and immediately above waves, the resemblance to the usual boundary layer disappears completely. Far from the surface the wave-induced fluctuations are attenuated, and in the case of stationary, horizontal homogeneity and neutral stratification, the boundary layer above the waves is very close to that above a solid flat surface up to a height where the Coriolis effects are significant. In particular, the turbulent momentum flux is constant with height and the wind profile is nearly logarithmic. The drag coefficient (and, therefore, the effective roughness parameter) is formed jointly by all drag mechanisms arising in the relatively thin layer near the interface.

It is known that the concept of the stationary boundary layer above the sea is not adequate (see e.g., Benilov *et al.*, 1978). In the case of the Pierson-Moskovitz spectrum, it is possible to estimate the height h_{en} of the boundary layer whose total kinetic energy is equal to the energy of a fully developed sea

$$h_{en} \propto 10\frac{u^2}{g},$$

where u is the velocity scale and g is the acceleration of gravity. Obviously, h_{en} may reach several hundred meters. It is not yet clear whether a saturated wave spectrum exists for constant wind. However, observations show that the growth rate of sea waves with constant wind diminishes and it is reasonable to consider a statistically equilibrium state. Under non-stationary conditions, development of

Boundary-Layer Meteorology **63**: 65–96, 1993.

the boundary layer causes slow evolution of the wind velocity and vertical momentum flux profiles. As will be shown below, another reason for nonstationarity may be imbalance between outer wind stress and wave-produced stress.

The main problem in the theory of the boundary layer is to establish a relation between turbulent stress $\mathbf{T}$ and wind velocity vector $u = (u, v)$ at arbitrary height z

$$\mathbf{T} = \rho_a C|\mathbf{u}|\mathbf{u}, \tag{1}$$

where ρ_a is air density and C is the drag coefficient at height z.

The value of C for neutral stratification above land depends on the only morphological surface characteristic, the roughness parameter z_0, which is connected with C by the relation

$$C = \left(\frac{k}{\ln(z/z_0)}\right)^2, \tag{2}$$

where k is von Karman's constant.

The sea surface state is not predetermined due to waves produced by local wind and swell. In this case, z_0 is usually estimated with the help of the famous formula suggested by Charnock (1955)

$$z_0 = mv_*^2/g, \tag{3}$$

where v_* is the friction velocity and m is an empirical coefficient whose value varies from 0.01 to 0.05. It is well known that the expression on the right side of (3) gives a very good scale for the roughness parameter. However, we can consider this formula only as a qualitative relation because the scatter of empirical data is very large. This discrepancy may be explained by the obvious inaccuracy of determination of z_0 as well as by the influence of nonstationarity, nonhomogeneity and density stratification. The scatter may be explained also by a variety of wave situations which are often far from conditions for which relation (3) is valid. This additional scatter may arise due to systematic deviations of the wind profile from a logarithmic one maintained by wave-produced momentum fluxes. Formula (3) appears to operate in the case of a fully developed sea without swell. The coefficient has been estimated to be 0.0130 by Smith and Banke (1975), 0.0144 by Garratt (1977), and 0.0185 by Wu (1980).

The value of v_* is usually unknown; however, relations (2) and (3) allow formulation of the drag law as follows

$$\ln\frac{\mathbf{u}^2}{gz} = -\ln(mC) - \frac{k}{\sqrt{C}}, \tag{4}$$

which connects the drag coefficient with the wind velocity at any height.

Expression (4) gives a rather weak dependence of C on wind velocity. Thus, for $m = 0.0185$, Wu (1980) suggested the approximation

$$C_{10} = (0.80 + 0.065\mathbf{u}_{10})10^{-3}. \tag{5}$$

According to the empirical data of Donelan (1982), this relation is valid in the case of a developed sea ($u_{10}/c_o \in (0.8, 1.5)$, where c_p is the phase velocity of the spectrum peak frequency), but underestimates C_{10} considerably at limited fetches (see Figure 8 below).

In the general case, the drag coefficient is a function of the 2–D wave spectrum

$$C = C\left(\frac{u^2}{gz}, S(\omega, \theta)\right). \tag{6}$$

In a number of works, relations between the drag coefficient C and wind wave parameters have been derived. But in the majority of papers, the structure of the wave boundary layer and the mechanisms of drag formation have not been taken into account. These papers are mostly devoted to the generalization of empirical data. Until now, it is not yet clear what contributions are made by different parts of the wave spectrum (see Toba *et al.*, 1990). The most powerful method to investigate the drag formation mechanism is numerical two- and three-dimensional modeling of the statistical structure of the wave boundary layer (Chalikov 1976, 1978, 1986), which will be discussed in this paper. The potential of this method has not been fully exploited so far; however, this approach is too complicated to be used in parameterization schemes for joint atmosphere-sea models. It seems natural to base such schemes on the one-dimensional approach taking into account specific properties of the wave boundary layer.

This problem was considered by Janssen (1989, 1991), where an attempt was made to investigate the spectral mechanism of drag formation as well as the direct and inverse coupling between wind and waves. The approaches demonstrated in these articles are different. In the first case where calculations were made of the wave-produced momentum fluxes, the author used the quasilaminar Miles' theory in terms of a "wave diffusion coefficient". It is unlikely that this effect may be represented using some sort of local diffusion coefficient, which assumes that the flux of momentum is created by the velocity profile. Wave-produced momentum flux is formed not by the wind itself but by externalities such as the moving water surface. Janssen used a nondivergent form of the diffusion term that resulted in some contradictions. To obtain the wave-produced momentum flux, Janssen (1989) performed integration of the momentum flux spectral density over frequency to infinity. It is incorrect because the spectrum and the wind-wave interaction parameter are unknown for large frequencies. In Janssen (1990), the logarithmic wind profile was used jointly with a formula for the roughness parameter taking into account the wave-produced effect. This formula was obtained incorrectly (see Chalikov, 1992).

Chalikov and Makin (1991) suggested a 1-D model where the vertical wave-induced momentum flux profile integrated over all frequencies has been approximated by the step-function whose parameters have been chosen with respect to

results of the numerical experiments with the 2–D model. The model equations allowed an analytical solution which gave a relation between the drag coefficient and the non-dimensional fetch $\tilde{x} = xg/v_*^2$ (or non-dimensional peak frequency $\tilde{\omega}_p = \omega_p v_*/g$). It has been shown that the drag coefficient may change by a factor of 2 to 4 depending on the fetch, quite in accordance with Donelan's data (1982).

In this paper we shall discuss a new version of the 1-D model where the main drag mechanisms arising above the wave surface are taken into account. Examples of the calculations for growing waves in the absence of swell will be given.

2. 2–D Model of the Wave Boundary Layer

Consider the Reynolds equations in the coordinate system $(x = (x, y), \zeta = z - \eta)$ connected with the sea-surface $\eta(t, \chi)$

$$\frac{\partial \mathbf{u}}{\partial t} + \frac{\partial}{\partial \mathbf{x}_j}(\mathbf{u}u_j + \overline{\mathbf{u}'u_j'}) + \nabla p + \frac{\partial}{\partial \zeta}\left(\mathbf{u}W + \overline{\mathbf{u}'w'} - \frac{\partial \eta}{\partial x_j}\overline{\mathbf{u}'u_j'} + p\nabla\eta\right) = 0, \tag{7}$$

$$\frac{\partial w}{\partial t} + \frac{\partial}{\partial x_j}(wu_j + \overline{w'u_j'}) + \frac{\partial}{\partial \zeta}\left(wW + \overline{w'w'} - \frac{\partial \eta}{\partial x_j}\overline{w'u_j'} + p\right) = 0, \tag{8}$$

$$\frac{\partial u_j}{\partial x_j} + \frac{\partial W}{\partial \zeta} = 0. \tag{9}$$

Here t is time, $x = (x_1, x_2)$ are horizontal coordinates; ζ is vertical coordinate, $\eta(t, x)$ is surface elevation, coinciding with the lower bound $\zeta = 0$; $u = (u_1, u_2)$ is the horizontal and W the vertical velocity, p is dynamic pressure divided by ρ_a, $\nabla \equiv (\partial/\partial x_1, \partial/\partial x_2)$, $j = 1, 2$. The summation convention is used. W is the contravariant vertical velocity (hereafter $\langle\langle\cdot\rangle\rangle$ means the inner product of two vectors):

$$W = w - \frac{\partial \eta}{\partial t} - \mathbf{u}\cdot\nabla\eta. \tag{10}$$

Equations (7)–(9) were derived by a special averaging procedure applied to the equations of motion written in the ζ-system of coordinates (Chalikov, 1978, 1980).

At the upper bound $\zeta = h$, either the wind velocity $\mathbf{u} = \mathbf{u}_h$ or the vertical momentum flux T_h

$$\mathbf{T}_h = \mathbf{u}W + \overline{\mathbf{u}'w'} - \frac{\partial \eta}{\partial x_j}\overline{\mathbf{u}'u_j'} + p\nabla\eta \tag{11}$$

is given.

At the lower bound $\zeta = 0$, the surface velocity components are known

$$\mathbf{u} = \mathbf{u}_0(t, \mathbf{x}), \qquad w = w_0(t, \mathbf{x}), \tag{12}$$

and they must satisfy the surface kinematic condition

$$\frac{\partial \eta}{\partial t} + \mathbf{u} \cdot \nabla \eta - w_0 = 0. \tag{13}$$

Expression (13) yields W_0 and the advective vertical momentum flux equals zero. Conditions (12) are rather restrictive for computation because when $\zeta \to 0$, the discretization step $\Delta\zeta$ must be of order z_0. Furthermore, with decreasing ζ, the role of short waves increases. The necessity for their resolution leads to a small horizontal step. That is why it is better to locate the lower bound at some small height ζ_r and to use a parameterization of surface stress in the form of the quadratic drag law

$$\overline{\mathbf{u}' w'} - \frac{\partial \eta}{\partial x_j} \overline{\mathbf{u}' u_j'} = C_r |\Delta \mathbf{u}| \, \Delta \mathbf{u} \tag{14}$$

$$\overline{w' w'} - \frac{\partial \eta}{\partial x_j} \overline{w' u_j'} = C_r |\Delta \mathbf{u}| \, \Delta w. \tag{15}$$

Here $\Delta \mathbf{u} = \mathbf{u}_r - \mathbf{u}_0$, $\Delta w = w_r - w_0$, and the index r corresponds to $\zeta = \zeta_r$.

Elimination of the domain $\zeta < \zeta_r$, where the quadratic drag law is introduced, excludes high-frequency waves with $\omega > \omega_r = \sqrt{2\pi g/\zeta_r}$ from consideration.

To close Equations (7) and (8), the second-order moments are written in terms of the velocity deformation tensor, mixing-length

$$l = k\zeta, \tag{16}$$

turbulent viscosity coefficient K, and turbulent energy e. The latter is calculated using standard non-stationary equations written in the $(\mathbf{x}, \zeta)$ coordinate system.

Discussion and analysis of Equations (7)–(9) as well as the main results obtained by 1985 have been presented in an overview paper of Chalikov (1986). The latest results based on this approach have been given by Makin and Burgers (1992).

In the case of a single-mode surface wave with phase velocity c, the problem may be reduced to a stationary one with the use of a moving coordinate system $\mathbf{x} = \mathbf{x} - ct$. When the surface form is the sum of a number of dispersing waves, the problem becomes essentially non-stationary.

3. The Wind-Wave Interaction Parameter, Momentum and Energy Exchange Between Wind and Waves

The extensive computations of the statistical structure above monochromatic and multi-mode surfaces based on Equations (7)–(9) have been performed. They yielded, in particular, the wind-wave interaction parameter

$$\beta(\omega) = \frac{\rho_a}{\rho_w} \frac{\epsilon(\omega)}{\omega S(\omega)}, \tag{17}$$

where ϵ is the spectral density of energy exchange divided by air density ρ_a, $S(\omega)$ is the wave spectrum, ρ_w is water density. The interaction parameter β can be approximated as

$$10^4\,\beta = \begin{cases} -a_1\tilde{\omega}_a^2 - a_2, & \tilde{\omega}_a < -1 \\ a_3\,\tilde{\omega}_a(a_4\tilde{\omega}_a - a_5) - a_6, & \tilde{\omega}_a \in (-1, \Omega_1/2) \\ (a_4\tilde{\omega}_a - a_5)\,\tilde{\omega}_a, & \tilde{\omega}_a \in (\Omega_1/2, \Omega_1) \\ a_7\tilde{\omega}_a - a_8, & \tilde{\omega}_a \in (\Omega_1, \Omega_2) \\ a_9(\tilde{\omega}_a - 1)^2 + a_{10}, & \tilde{\omega}_a > \Omega_2. \end{cases} \tag{18}$$

Here, $\tilde{\omega}_a = \omega|\mathbf{u}_\lambda|\cos\theta/g$ is the non-dimensional "apparent" frequency of a wave moving at an angle θ to wind direction; $\mathbf{u}_\lambda$ is wind velocity at a height equal to the "apparent" wavelength $\lambda_a = 2\pi g/(\omega^2|\cos\theta|)$; $a_1 - a_{10}$ and Ω_1, Ω_2 are parameters depending on the drag coefficient at height $\zeta = \lambda_a$:

$$\begin{aligned} \Omega_1 &= 1.075 + 75\,C_1, & \Omega_2 &= 1.2 + 300C_1, \\ a_1 &= 0.25 + 395C_1, & a_3 &= (a_0 - a_2 - a_1)/(a_0 + a_4 + a_5), \\ a_2 &= 0.35 + 150C_1, & a_5 &= a_4\Omega_1, \\ a_4 &= 0.30 + 300C_1, & a_6 &= a_0(1 - a_3), \\ a_9 &= 0.35 + 240C_1, & a_7 &= (a_9(\Omega_2 - 1)^2 + a_{10})/(\Omega_2 - \Omega_1), \\ a_{10} &= -0.06 + 470C_1, & a_8 &= a_7\Omega_1, \\ & & a_0 &= 0.25\,a_5^2/a_4. \end{aligned}$$

Examples of the $\beta(\tilde{\omega}_a)$-relation for different values of the drag coefficient C_1 are shown in Figure 1. Note that at high frequencies $|\tilde{\omega}_a| \geq 2$, the, β-parameter is proportional to $\tilde{\omega}_a^2$, i.e., the energy flux depends on the squared wind velocity. This dependence, confirmed by experimental data of Hsiao and Shemdin (1983), seems to be more natural than the linear one derived from field experimental data (see Snyder *et al.*, 1981). High frequency waves are nearly "fixed" with respect to wind; thus their drag in turbulent flow is likely to have a quadratic dependence on wind velocity as is the case of usual roughness elements.

The linear dependence on $\tilde{\omega}_a$ exists only in the vicinity of $\tilde{\omega}_a \simeq 1$. Note that when $\tilde{\omega}_a \leq 1$, the value of β is negative. This case corresponds either to waves runing faster than the wind or to waves moving at angles $\theta > \pi/2$ to the wind. In either case, the waves give their energy back to wind. In particular, the waves directed strictly perpendicular to the wind are moving in "motionless" media. Hence, the turbulent viscosity is supported by the wind blowing along the wave crests. The momentum transferred from the waves to the wind reduces the momentum exchange. So, this situation is essentially non-steady. However, the majority of the momentum leads to an increase of boundary-layer height. The time scale of this adaptation is large enough to make the inverse fluxes of momentum and energy important factors in stabilization of the wave spectrum.

In the scheme described above, the values of $\mathbf{u}_1$ and C_1 are computed at a

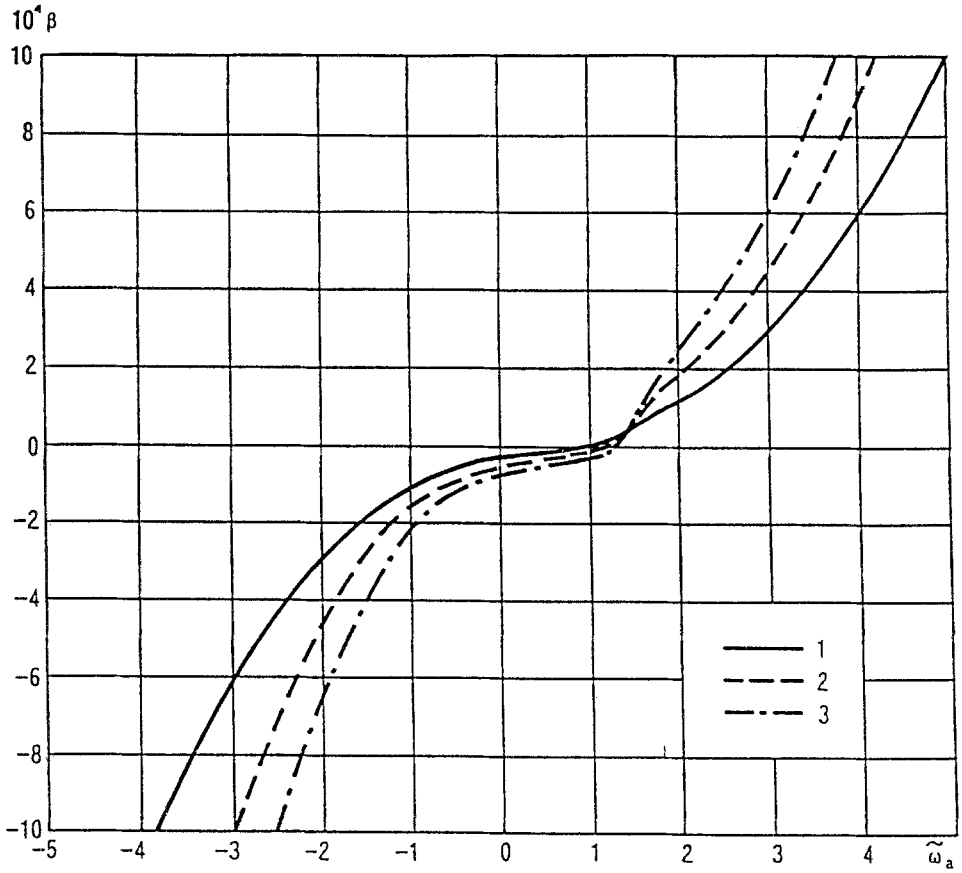

Fig. 1. Dependence of interaction parameter β on the "apparent" frequency $\tilde{\omega}_a = \omega|\mathbf{u}_\lambda| \cos\theta/g$ for different values of the drag coefficient C_λ (formulas (18), (19)): $1 - C_\lambda = 10^{-3}$, $2 - C_\lambda = 2 \cdot 10^{-3}$, $3 - C_\lambda = 3 \cdot 10^{-3}$.

height equal to the apparent wave length λ_a. Since the wind velocity and drag coefficient change with height, introduction of $\mathbf{u}_\lambda$ and C_λ eliminates the uncertainty in choosing a reference level, which is inherent in all schemes of β evaluation. This allows not only a reduction of the number of governing parameters, but also corresponds to the physical essence of the process, because with increasing frequency, the height of the layer where the wind-wave interaction takes place becomes thinner. In other words, everything outside this layer is insignificant for a given wave. This interpretation of the β-parameter allows one to consider the superposition of momentum fluxes produced by different modes in a most natural manner.

Applying the scheme in question to spectral computations of energy and momentum fluxes exchanges, it is possible in the first approximation to suggest that the wind profile is logarithmic with a certain total roughness parameter

$$\mathbf{u}(\lambda_a) = \mathbf{u}_h \frac{\ln(\lambda_a/z_0)}{\ln(h/z_0)}. \tag{20}$$

Here, $\mathbf{u}_h$ is the wind velocity at height h. Then,

$$C_\lambda = \left(\frac{k}{\ln(\lambda_a/z_0)}\right)^2. \tag{21}$$

In fact, the total roughness parameter for an arbitrary wave field is not known; moreover, the wave drag produces a deviation of the wind profile from the logarithmic one. That is why the simplified method may be inaccurate, especially for high frequencies as well as for small heights.

The empirical data on the wind-wave interaction parameter collected by Plant (1982) are shown in Figure 2 together with the (dependencies (equations 18, 19) computed for different C_1. The scatter is very large, one order of magnitude. Obviously, a considerable part of this scatter may be explained taking into account the additional dependence on C_λ. It is interesting that for $\tilde{\omega} > 0.1$, both the empirical data and our approximation exhibit the quadratic dependencies of β on $\tilde{\omega}$

In a recent paper, van Duin and Janssen (1992) noted that turbulent nonlinear models "showed a substantial disagreement with observed growth rates for both high and low-frequency waves". A countervailing opinion is that the agreement between empirical data and the results obtained with a full nonlinear model is good, much better than that cited in the paper above. This is not surprising, because the model of Duin and Jansson (1992) in fact is a simplified version of Equations (7)–(9). Note that we did not use data collected by Plant (1982) for tuning the model and Figure 2 was included only in the latest version of this paper.

The energy flux E to a monochromatic wave with amplitude A and frequency ω running at an angle θ to the wind may be computed via the relation

$$E = \rho_w g \omega \frac{A^2}{2} \beta(\tilde{\omega}_a, C_\lambda). \tag{22}$$

The energy flux to a wave surface with spectrum $S(\omega)$ and angle distribution $D(\omega, \theta)$ is equal to

$$E = \rho_w g \int_0^{\omega_r} \int_{\pi}^{\pi} \epsilon(\omega, \theta)\, \mathrm{d}\theta\, \mathrm{d}\omega, \tag{23}$$

where $\epsilon(\omega, \theta) = \omega S(\omega) D(\omega, \theta) \beta(\tilde{\omega}_a, C_\lambda)$ is the spectral density of energy exchange.

Using the relation, valid for linear waves

$$\eta = -\frac{k}{\omega} \frac{\partial \eta}{\partial t},$$

it is possible to compute the momentum flux to a monochromatic wave

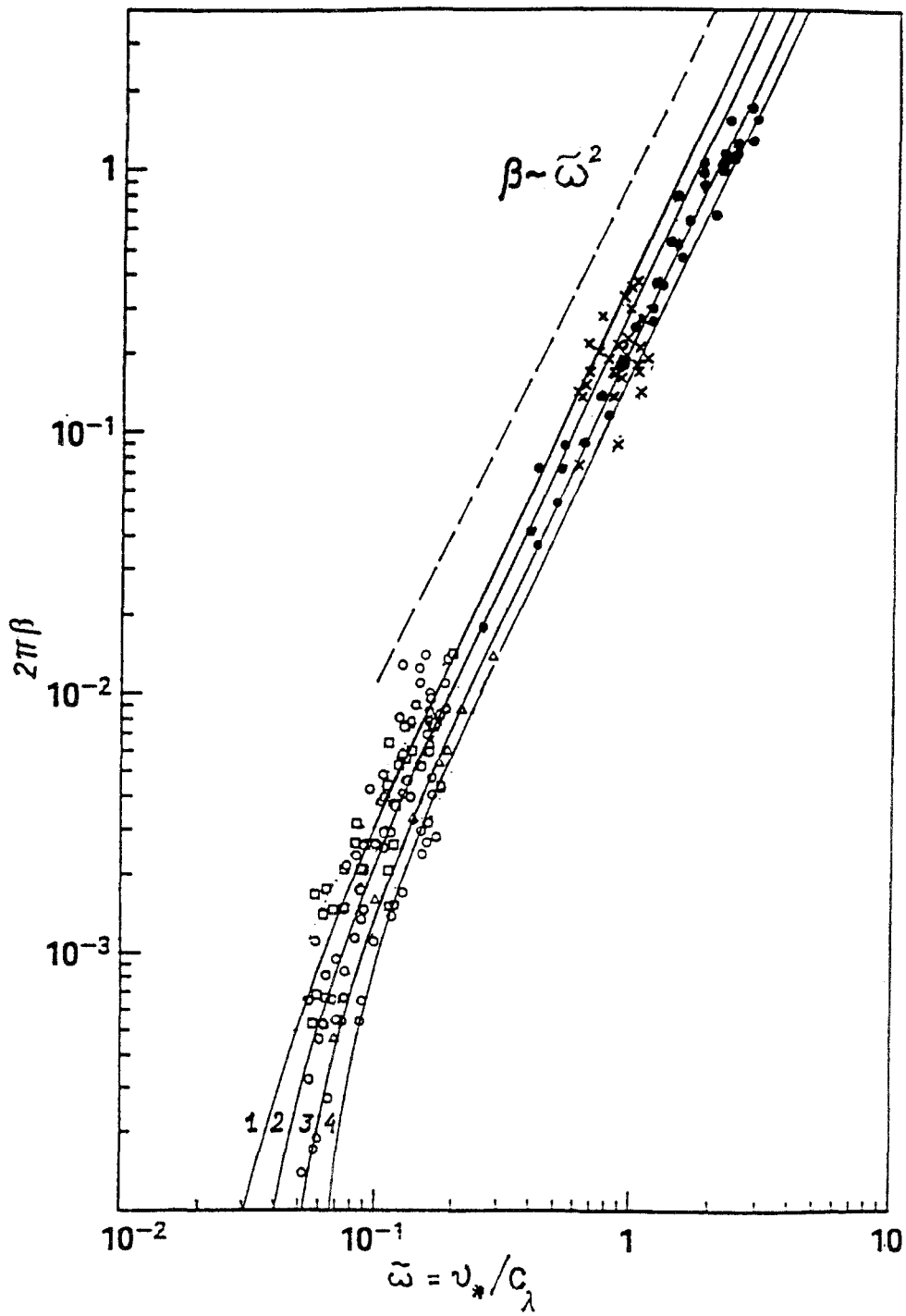

Fig. 2. Empirical data on the wind-wave interaction parameter β collected by Plant (1982). Solid lines represent the approximation (18), (19): $1 - C_\lambda = 0.75 \cdot 10^{-3}$; $2 - 2 \cdot 10^{-3}$, $3 - 3 \cdot 10^{-3}$, $4 \div 4 \cdot 10^{-3}$; dashed line – dependence $\beta \propto \omega^{-2}$.

$$\tau_0 = \langle p\nabla\eta\rangle = -\frac{k}{\omega}\langle p\frac{\partial\eta}{\partial t}\rangle = \rho_w g k\frac{A^2}{2}\beta(\tilde{\omega}_a, C_\lambda). \tag{24}$$

For an arbitrary wave surface, formula (24) may be generalized to

$$\tau_0 = \rho_w g\int_0^{\omega_r}\int_\pi^\pi \mathcal{F}(\omega,\theta)\,\mathrm{d}\theta\,\mathrm{d}\omega, \tag{25}$$

where $\mathcal{F}(\omega,\theta) = \mathbf{k}S(\omega)D(\omega,\theta)\beta(\tilde{\omega}_a, C_\lambda)$ is the spectral density of momentum exchange; $\mathbf{k} = (k_1, k_2)$, $k_1 = \omega^2/g\cos\theta$ and $k_2 = \omega^2/g\sin\theta$.

The upper limit of integration ω_r in integrals (23) and (25) prescribes the value at the lower level ζ_r of the numerical model. In fact, the energy flux and total drag are produced by all of the wave spectrum. However, expansion of the integration to infinity is impossible because neither the shape of the wave spectrum nor the interaction parameter β is known. Nevertheless, the computational error of the total energy flux due to the finiteness of ω_r is insignificant, because integral (23) converges rather quickly: as $S \propto \omega^{-5}$ and $\beta \propto \omega^2$, the integrand is proportional to ω^{-2}. At the same time, integral (25) does not converge due to the incorrect extension of $\beta(\omega)$ and $S(\omega)$ to infinity. So, introduction of an upper limit ω_r in this case is absolutely necessary. The wave drag produced by waves with frequencies $\omega > \omega_r$ is described using the quadratic drag law (14), (15).

In any case, the divergence of integral (25) indicates that wave drag formation may depend strongly upon the high-frequency frequency spectrum band.

4. A 1-D Model of the Wave Boundary Layer (WBL)

In order to derive non-dimensional model equations, let us consider the horizontal averaging operator

$$\langle a\rangle = \frac{1}{L_1L_2}\int_0^{L_1}\int_0^{L_2} a\,\mathrm{d}x_1\,\mathrm{d}x_2.$$

Then the averaged Equations (7)–(9) become

$$\frac{\partial\langle\mathbf{u}\rangle}{\partial t} + \frac{\partial}{\partial\zeta}\left\langle \mathbf{u}W + \overline{\mathbf{u}'w'} - \frac{\partial\eta}{\partial x_j}\overline{\mathbf{u}'u_j'} + p\nabla\eta\right\rangle = 0, \tag{26}$$

$$\frac{\partial\langle w\rangle}{\partial t} + \frac{\partial}{\partial\zeta}\left\langle wW + \overline{w'w'} - \frac{\eta}{x_j}\overline{w'u_j'} + p\right\rangle = 0, \tag{27}$$

$$\frac{\partial\langle W\rangle}{\partial\zeta} = 0. \tag{28}$$

Equation (28) and kinematic condition (10) yields $\langle W\rangle = 0$ at any height; $\langle\eta\rangle = 0$ by definition.

Equation (27) characterizes the non-static rate of flow and is of less interest to us. Equation (26) describes the momentum balance. The terms in angle brackets

are the components of the vertical momentum flux: the first is produced by wave-induced velocity; the second, by turbulence; the third, by wave-induced variations of the longitudinal momentum flux; and the fourth by wave-induced variations of pressure. The vertical distributions of these quantities have been investigated by Makin and Chalikov (1986a, 1986b), and Makin (1989).

As the relaxation time scale of the boundary layer, with depth of order of several tens of meters, does not exceed 10^2–10^3 sec (approximately one order smaller than the time scale of wave field development), Equation (26) may be written in the form of a stationary balance of momentum

$$\frac{\partial}{\partial \zeta}(\mathbf{T} + \tau) = 0, \tag{29}$$

where $\mathbf{T}$ is the vertical momentum flux vector produced by turbulence

$$\mathbf{T} = \left\langle \overline{\mathbf{u}' w'} - \frac{\partial \eta}{\partial x_j} \overline{\mathbf{u}' u_j'} \right\rangle, \tag{30}$$

and τ is the wave-induced flux produced by wave fluctuations of velocity and pressure

$$\tau = \langle \mathbf{u} W + p \nabla \eta \rangle. \tag{31}$$

When $\zeta \to 0$, the contravariant component W diminishes, and the momentum flux to a wave is, in practice, transferred by surface pressure only

$$\tau_0 = \langle p \nabla \eta \rangle. \tag{32}$$

The turbulent flux of momentum at the surface $\zeta = 0$ is equal to

$$\mathbf{T}_0 = \langle C_r \Delta \mathbf{u}_r \mathbf{u}_r \rangle. \tag{33}$$

This momentum flux generates an average horizontal flow in water, i.e., currents.

Note that from the point of view of boundary-layer theory itself, it is impossible to break up the total flux into a flux to waves and that to the current, because their relationship depends on an arbitrary scale ζ_r as well as on the available horizontal resolution of the numerical model. If we are to take into consideration all possible scales up to the molecular viscosity range, then the momentum is transferred to all surface perturbations almost by pressure alone, and the longitudinal flow is generated only by molecular friction. Introducing the discretization scale ζ_r increases the currentward part of momentum because the subgrid waves are omitted from consideration. The wave part of the momentum decreases accordingly. The sum of these fluxes must be conserved.

There is no contradiction in this uncertainty. In fact, the overwhelming part of the momentum is transferred to all wave frequencies by the form drag. However, all waves finally vanish and their momentum passes to currents. Besides, the lifetime of very short waves is small and that of long waves is so large that they

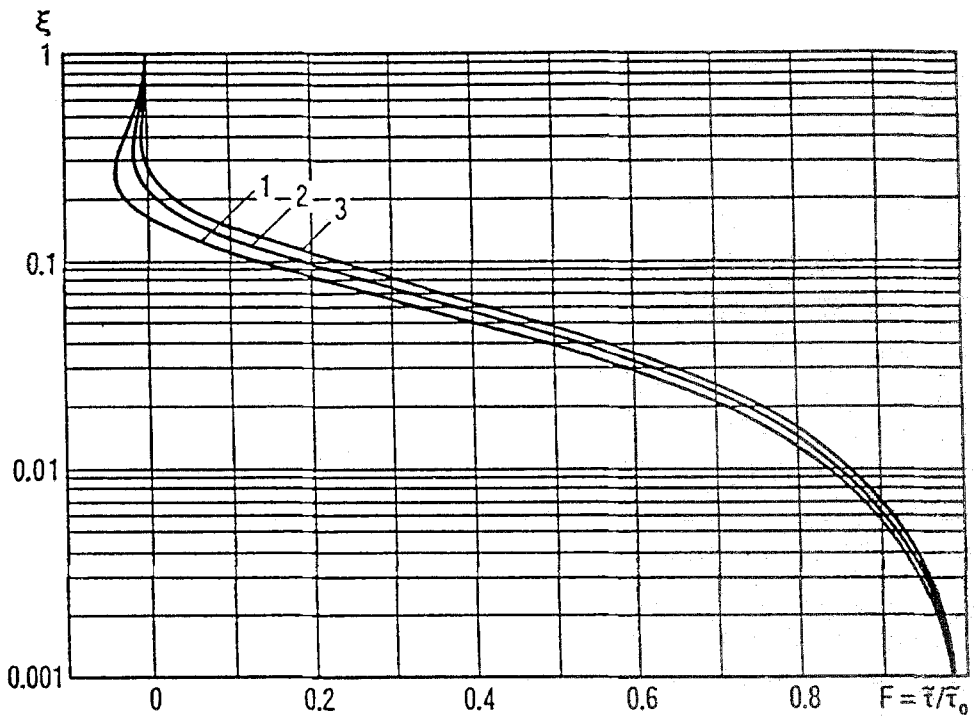

Fig. 3. Examples of vertical distribution of momentum flux $F = |\tau|/|\tau_0|$ produced by a monochromatic wave: $1 - C_\lambda = 10^{-3}$, $2 - C_\lambda = 2 \cdot 10^{-3}$, $3 - C_\lambda = 3 \cdot 10^{-3}$.

can even reach the shore. So, the possibility of the separation mentioned above depends on the time and horizontal scales of wave energy dissipation as well.

To construct a 1-D model of a wave boundary layer, it is necessary to define the vertical distribution of wave-induced momentum flux $\tau(\zeta)$. For monochromatic waves running at an angle θ to the wind, the vertical distribution of $\tau(\zeta)$ may be taken in the form

$$\tau = \tau_0 F(\tilde{\omega}_a, C_\lambda, \xi), \tag{34}$$

where F is a function depending on non-dimensional frequency $\tilde{\omega}_a$, drag coefficient C_λ at height $\zeta = \lambda_a$ and the non-dimensional height $\xi = \zeta/\lambda_a$; τ_0 is the surface wave-induced momentum defined by (25).

The scalar function F was repeatedly investigated in numerical experiments with the 2–D model. The examples of this function are shown in Figure 3 for different values of C. Our approximation of this function is based on computations performed by Makin (1989). They are given by the following expression

$$F = \left(1 - \frac{\xi}{\xi_0}\right) e^{-10\xi}, \tag{35}$$

where ξ_0 is a function of drag coefficient C_λ, and $\xi_0 = 0.31 - 50 C_\lambda$. It is interesting

to note that F is in practice independent of $\tilde{\omega}_a$. This means that the frequency exerts an influence upon the surface momentum flux τ_0, but not upon its vertical distribution on the scale z/λ_a. We suppose that in the case of the multi-mode surface, $\tau(\zeta)$ can be expressed by superposition of the "elementary" fluxes:

$$\tau = \rho_w g \int_0^{\omega_r} \int_{\pi}^{\pi} \mathbf{k} S(\omega) D(\omega, \theta) \beta(\tilde{\omega}_a, C_\lambda) F(\xi, C_\lambda) \, \mathrm{d}\theta \, \mathrm{d}\omega. \tag{36}$$

Let h be the height where the wave disturbances vanish and $\mathbf{T}_h$ is equal to pure turbulent momentum flux. Let us then introduce the non-dimensional variables marked with a tilde, using the following scales: for velocity,

$$v_* = \sqrt{|T_h|/\rho_a}; \tag{37}$$

for time, v_*/g; for length (height), v_*^2/g; for frequency, g/v_*; and for wave number, g/v_*^2. Now, using an assumed closure hypothesis, we can write equation (29) as follows:

$$\frac{\partial}{\partial \tilde{\zeta}} \left(\tilde{K} \frac{\partial \tilde{\mathbf{u}}}{\partial \tilde{\zeta}} + \tilde{\tau} \right) = 0, \tag{38}$$

where $\tilde{K} = Kg/v_*^3$ is a non-dimensional turbulent viscosity coefficient. On the upper bound we assume

$$\tilde{\zeta} = h: \qquad \tilde{K} \frac{\partial \tilde{\mathbf{u}}}{\partial \tilde{\zeta}} + \tilde{\tau} = \tilde{\mathbf{T}}_h. \tag{39}$$

Note that on the upper bound, $|\tau| \ll |\mathbf{T}_h| \simeq 1$. Integrating (38) over the range $(\tilde{\zeta}, h)$ yields the equation

$$\tilde{K} \frac{\partial \tilde{\mathbf{u}}}{\partial \tilde{\zeta}} + \tilde{\tau} = \tilde{\mathbf{T}}_h, \tag{40}$$

which shows that the balance of momentum in the boundary layer is possible only when the vector of total momentum stress at the surface $\tilde{\zeta} = 0$ is equal to the outer momentum stress $\tilde{\mathbf{T}}_h$. In particular, this approach is possible in a symmetric angular wave distribution, that is, when $D(\omega, \theta) = D(\omega, -\theta)$. Otherwise, the non-balanced lateral constituent of stress leading to a non-stationary regime may arise.

To close Equation (40), we shall use the same scheme as in the 2–D case, i.e.

$$\tilde{K} = \tilde{l} \nabla \sqrt{\tilde{e}/c_1}, \tag{41}$$

where $\tilde{l}$, $\tilde{e}$ are the non-dimensional mixing length and turbulent energy, $c_1 \simeq 4.6$ – an empirical constant. Let us assume linear dependence of the mixing length upon the distance to the surface

$$\tilde{l} = k\tilde{\zeta}, \tag{42}$$

Turbulent energy $\tilde{e}$ satisfies the equation

$$\tilde{P} + \frac{\partial}{\partial \tilde{\zeta}} \tilde{K} \frac{\partial \tilde{e}}{\partial \tilde{\zeta}} - \frac{(\tilde{e}/c_1)^{3/2}}{\tilde{l}} = 0. \tag{43}$$

Here, $\tilde{P}$ is the non-dimensional production of turbulent energy and the last two terms describe diffusion and dissipation of $\tilde{e}$, accordingly. To obtain $\tilde{P}$, let us consider the mean energy equation, taking an inner product of (38) and $\tilde{\mathbf{u}}$

$$\frac{\partial}{\partial \tilde{\zeta}} \left(\left(\tilde{K} \frac{\partial \tilde{\mathbf{u}}}{\partial \tilde{\zeta}} + \tilde{\tau} \right) \cdot \tilde{\mathbf{u}} \right) - \left(\tilde{K} \frac{\partial \tilde{\mathbf{u}}}{\partial \tilde{\zeta}} + \tilde{\tau} \right) \cdot \frac{\partial \tilde{\mathbf{u}}}{\partial \tilde{\zeta}} = 0. \tag{44}$$

The first term corresponds to turbulent flux and transport (by wave-induced fluctuations) of mean kinetic energy $\tilde{E}_m$. The second describes the transformation of $\tilde{E}_m$ to turbulent energy $\tilde{e}$ and the mutual transformation of energy $\tilde{E}_m$ and kinetic energy of wave-induced fluctuations $\tilde{E}_w$, correspondingly. The discussion on energetic properties of the wave boundary layer has been given by Panchenko and Chalikov (1984).

The wave fluctuations redistribute $\tilde{E}_w$ slightly, but most of $\tilde{E}_w$ transforms to $\tilde{e}$ locally, so the production of $\tilde{e}$ may be assumed in the form

$$\tilde{P} = \left(\tilde{K} \frac{\partial \tilde{\mathbf{u}}}{\partial \tilde{\zeta}} + \tilde{\tau} \right) \cdot \frac{\partial \tilde{\mathbf{u}}}{\partial \tilde{\zeta}} \tag{45}$$

or, taking into account (40),

$$\tilde{P} = \tilde{\mathbf{T}}_h \cdot \frac{\partial \tilde{\mathbf{u}}}{\partial \tilde{\zeta}}, \tag{46}$$

where $\tilde{\mathbf{T}}_h$ is constant with height.

Hence, the turbulent energy $\tilde{e}$ is the solution of the following equations:

$$\tilde{\mathbf{T}}_h \cdot \frac{\partial \tilde{\mathbf{u}}}{\partial \tilde{\zeta}} + \frac{\partial}{\partial \tilde{\zeta}} \tilde{K} \frac{\partial \tilde{e}}{\partial \tilde{\zeta}} - \frac{(\tilde{e}/c_1)^{3/2}}{\tilde{l}} = 0, \tag{47}$$

$$\tilde{\zeta} = \tilde{h}: \quad \tilde{e} = c_1, \qquad \tilde{\zeta} = \tilde{\zeta}_r: \quad \frac{\partial \tilde{e}}{\partial \tilde{\zeta}} = 0. \tag{48}$$

The first boundary condition implies that $\tilde{e}$ is constant above the wave boundary layer, the second one means that at a small height $\tilde{\zeta} = \tilde{\zeta}_r$, the dissipation of $\tilde{e}$ is balanced by its production.

The uncertainty of the roughness parameter z_0 is a specific feature of the wave boundary layer in contrast to the ordinary one. Moreover, we cannot localize the lower boundary too close to the surface, i.e., to the domain of influence of very short surface disturbances because the profile of the wave-induced momentum flux is unknown at small distance to the surface. That is why we must choose the lower boundary condition at some finite height where the influence of these disturbances vanishes.

We proceed from the assumption that in a sufficiently broad interval $(\tilde{\omega}_1, \tilde{\omega}_2)$, the frequency spectrum shape $\tilde{S}(\tilde{\omega})$ fits Phillips' law

$$\tilde{S}(\tilde{\omega}) = \alpha \tilde{\omega}^{-5}. \tag{49}$$

The non-universal part of the spectrum corresponding to a given wave situation is located below $\tilde{\omega}_1$. Above $\tilde{\omega}_2$, the effects of capillarity and other unknown phenomena occur. It is quite reasonable to choose the height $\tilde{\zeta}_r$ in the interval

$$\tilde{\zeta}_r \in \left(\frac{2\pi}{\tilde{\omega}_2^2}, \frac{2\pi}{\tilde{\omega}_1^2}\right), \tag{50}$$

where we assume the usual drag law to be appropriate

$$C_r = \left(\frac{k}{\ln(\tilde{\zeta}_r/\tilde{\zeta}_0)}\right)^2. \tag{51}$$

Here, $\tilde{\zeta}_0$ is the non-dimensional local roughness parameter which in the case of a developing sea is always smaller than the total one Eq. (3).

If the energy level in the Phillips interval does not depend on external conditions (such as wind velocity, fetch or spectrum shape at low frequencies), the value of the roughness parameter must be a universal characteristic of local drag. It has been known, however, that this parameter may change, for instance, with fetch. By analogy with a solid rough surface, we shall suppose that $\tilde{\zeta}_0$ is proportional to the root-mean-square height h_r of "rough elements", i.e., high-frequency waves

$$\tilde{\zeta}_0 \propto \tilde{h}_r, \tag{52}$$

where

$$\tilde{h}_r \propto \left(\int_{\tilde{\omega}r}^{\infty} \tilde{S}(\tilde{\omega})\, \mathrm{d}\tilde{\omega}\right)^{1/2}. \tag{53}$$

Using the Phillips spectrum Eq. (49), we obtain

$$\tilde{\zeta}_0 = \chi\sqrt{\alpha}, \tag{54}$$

where χ is a universal constant. As the mechanism of drag formation at high-frequency surface perturbations is unknown, this constant is to be derived from empirical data. An approximate estimation of χ is possible using the Pierson–Moskowitz spectrum with $\alpha = 8.1\,10^{-3}$. For $\tilde{z}_0 = m = 0.0130$ (Smith and Banke, 1975), 0.0144 (Garrat, 1977), 0.0185 (Wu, 1980), we have obtained $\chi = 0.14$, 0.16, 0.20, accordingly. As will be shown below, the wave-induced momentum flux for a developed sea is small, thus the wind profile is close to the logarithmic one even at a very small height. That is why we consider total and local roughness parameters to be equal to each other, i.e., $\tilde{z}_0 = \tilde{\zeta}_0$. For a developing sea, Janssen (1982) suggested

$$\alpha = 0.57\,\tilde{\omega}_p^{3/2}. \tag{55}$$

The computed vertical structure of the wave boundary layer for a developing sea (see below) shows fair agreement with empirical data (Donelan, 1982) for $\chi = 0.10$. So expression (4) takes the form

$$\ln\frac{\mathbf{u}^2}{g\zeta} = -\ln(0.1\sqrt{\alpha C}) - \frac{k}{\sqrt{C}}, \tag{56}$$

but this dependence (shown in Figure 7a) cannot be considerably better than formula (4) because both do not take into account the form drag produced by the overall spectrum. So formula (56) underestimates the drag coefficient, especially at small heights.

Finally, the lower boundary condition for Equation (40) is as follows

$$\tilde{\zeta} = \tilde{\zeta}_r: \qquad \tilde{\mathbf{T}}_R = \tilde{K}\frac{\partial\tilde{\mathbf{u}}}{\partial\tilde{\zeta}} = C_r|\tilde{\mathbf{u}}_r|\tilde{\mathbf{u}}_r. \tag{57}$$

Here, $\tilde{\mathbf{u}}_r$ is wind veloity at height $\tilde{\zeta} = \tilde{\zeta}_r$ and C_r is the local drag coefficient Eq. (51). The required $\tilde{\zeta}_0$ is computed according to Equation (54). The height $\tilde{\zeta}_r$ should be sufficiently small to describe the wave drag produced by the nonuniversal part of spectrum; i.e.,

$$\tilde{\zeta}_r \ll \frac{2\pi}{\tilde{\omega}_p^2}. \tag{58}$$

5. The Structure of the Boundary Layer Above Developing Waves

The 1-D model formulated above is intended for analysis of boundary-layer structure and for computing the energy and momentum fluxes to waves for an arbitrary 2–D wave spectrum and also for coupled WBL-wind wave mixed-layer modeling.

As an example, we consider the JONSWAP spectrum approximation for developing sea waves (Hasselmann *et al.*, 1973; Hasselmann *et al.*, 1980)

$$S(\tilde{\omega}) = \alpha\tilde{\omega}^{-5}\exp\left(-\frac{5}{4}\left(\frac{\tilde{\omega}}{\tilde{\omega}_p}\right)^{-4}\right)\gamma^G, \tag{59}$$

where $\gamma = 3.3$ and

$$G = \exp\left(-0.5\left(\frac{\tilde{\omega}-\tilde{\omega}_p}{\sigma\tilde{\omega}_p}\right)^2\right), \qquad \sigma = \begin{cases} 0.07, & \tilde{\omega}/\tilde{\omega}_p \le 1, \\ 0.09, & \tilde{\omega}/\tilde{\omega}_p > 1, \end{cases}$$

with directional distribution

$$D(\tilde{\omega}, \theta) = N_s^{-1} \cos^{2s}\left(\frac{\theta}{2}\right),$$

where

$$s = 9.77\left(\frac{\tilde{\omega}}{\tilde{\omega}_p}\right), \qquad \mu = \begin{cases} 4.06, & \tilde{\omega}/\tilde{\omega}_p \quad 1, \\ -2.34, & \tilde{\omega}/\tilde{\omega}_p > 1, \end{cases}$$

$$N_s = \int_{-\pi}^{\pi} \cos^{2s}\left(\frac{\theta}{2}\right) \mathrm{d}\theta = 2\sqrt{\pi}\frac{\Gamma(s+\frac{1}{2})}{\Gamma(s+1)},$$

where $\Gamma(s)$ is a gamma-function.

Due to the symmetric angular distribution D with respect to wind direction, we let the lateral stress component be equal to zero. In this case, the model equations can be written as

$$\tilde{K}\frac{\partial \tilde{u}}{\partial \tilde{\zeta}} + \int_0^{\tilde{\omega}_r}\int_{\pi}^{\pi} \mathbf{k} S(\tilde{\omega}) D(\tilde{\omega}, \theta) \beta(\tilde{\omega}_a, C_\lambda) F(\xi, C_\lambda) \,\mathrm{d}\theta \,\mathrm{d}\tilde{\omega} = 1, \tag{60}$$

$$\frac{\partial \tilde{u}}{\partial \tilde{\zeta}} + \frac{\partial}{\partial \tilde{\zeta}}\tilde{K}\frac{\partial \tilde{e}}{\partial \tilde{\zeta}} - \frac{(\tilde{e}/c_1)^{3/2}}{\tilde{l}} = 0, \tag{61}$$

where F, $\tilde{K}$ and $\tilde{l}$ are defined by Equations (35), (41), and (42), respectively. The boundary conditions are

$$\tilde{\zeta} = \tilde{\zeta}_r: \quad \frac{\partial \tilde{e}}{\partial \tilde{\zeta}} = 0, \quad \tilde{K}\frac{\partial \tilde{u}}{\partial \tilde{\zeta}} = C_r|\tilde{u}_r|\tilde{u}_r, \tag{62}$$

$$\zeta = h: \qquad \tilde{e} = c_1, \tag{63}$$

and $\tilde{\zeta}_r$ is chosen as

$$\tilde{\zeta}_r \ll \frac{2\pi}{\tilde{\omega}_p^2}, \qquad \tilde{\omega}_r = 15\,\tilde{\omega}_p. \tag{64}$$

Numerical integration of the above equations has been performed for a number of fetches defined by non-dimensional peak frequency $\tilde{\omega}_p$. The following values of $\tilde{\omega}_p$ were used: 0.06, 0.10, 0.15, 0.20.

The JONSWAP spectrum for different values of $\tilde{\omega}_p$ is shown in Figure 4a. The specific feature of this spectrum is a well pronounced overshoot effect; namely, the value of the spectrum for a smaller fetch exceeds that for a larger fetch for any given frequency $\tilde{\omega} > \tilde{\omega}_p$. This effect is described in the model in two ways. The main part of the spectrum for $0 < \tilde{\omega} < \tilde{\omega}_r$ is taken into account via the integral in equation (60). The influence of high frequency components is included in the local drag law Equation (62) using relations (51), (54), (55). The results are shown in Figures 4b, c and Figures 5, 6, 7.

Figure 4b shows the spectral density distribution of the momentum flux computed according to Equation (23). The density of the energy flux increases with

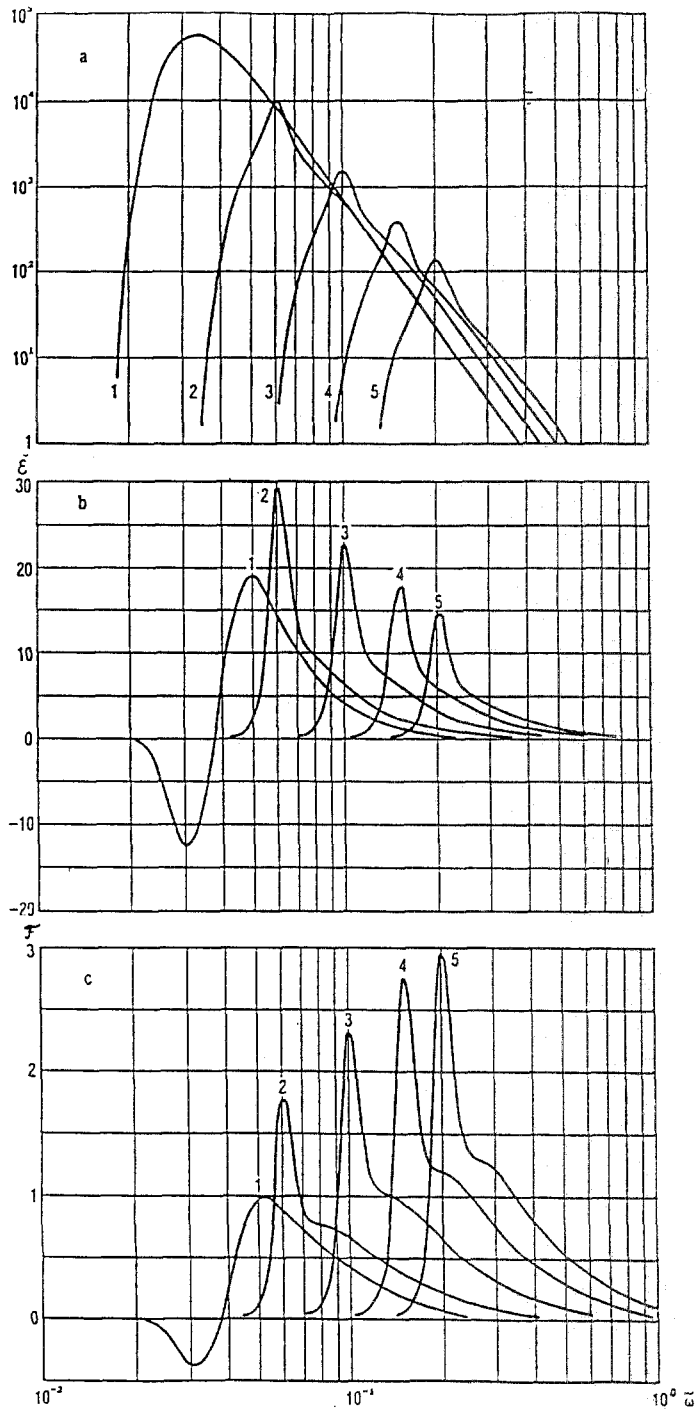

Fig. 4. (a) Wave spectra $\tilde{S}(\tilde{\omega})$; (b) wave energy flux density $\tilde{\epsilon}(\tilde{\omega})$; (c) wave momentum flux density $\tilde{\mathcal{F}}(\tilde{\omega}) = \tau_0(\tilde{\omega})$: 1 – $\tilde{\omega}_p = 0.033$ (Pierson-Moscowitz spectrum), 2 – $\tilde{\omega}_p = 0.06$, 3 – $\tilde{\omega}_p = 0.10$, 4 – $\tilde{\omega}_p = 0.15$, 5 – $\tilde{\omega}_p = 0.20$ (JONSWAP spectrum).

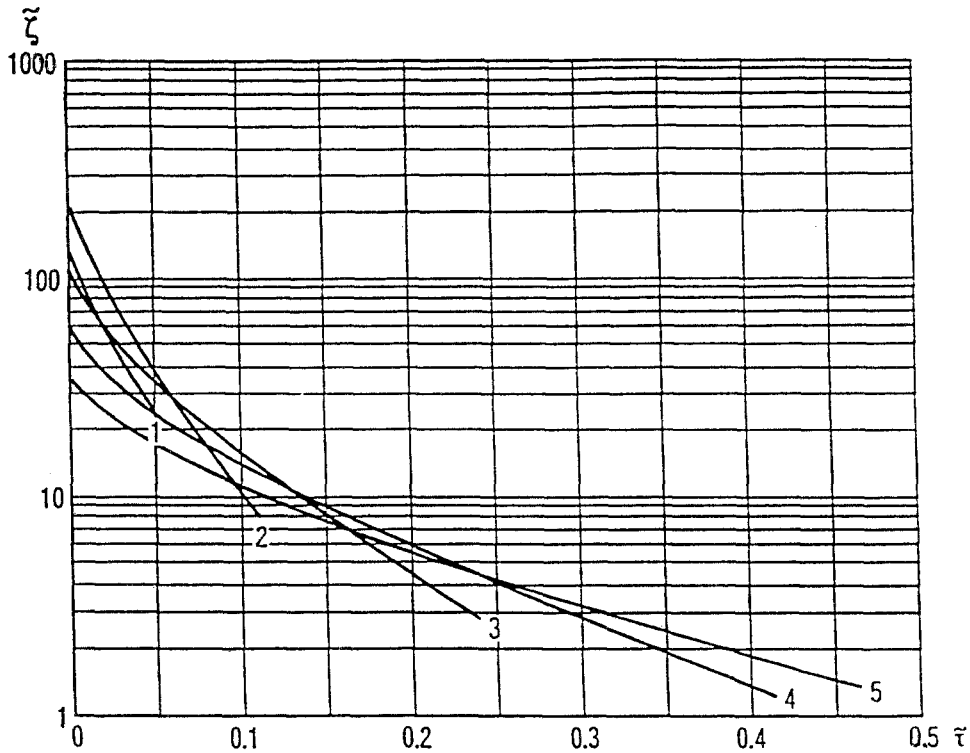

Fig. 5. Vertical distribution of momentum flux integrated over the spectrum $\tilde{\tau}$ (see (25)). Captions as in Figure 4.

increasing fetch, and its maximum is located in the vicinity of the peak frequency. It is remarkable that the spectral density of the momentum flux computed according to Equation (25) (Figure 4c) shows an inverse regularity: its maximum increases with decreasing fetch. This phenomenon may be explained by the overshoot effects, and partly by an increase in the local roughness parameter.

The vertical profiles of the wave-produced momentum flux computed by using (36) are shown in Figure 5. The larger the fetch, the smaller the flux, but the greater is the height that it reaches because it is produced by longer waves. In spite of the rapid vertical attenuation of the wave-induced flux of momentum at small fetches, the drag effects are stronger than at large fetches. This phenomenon may be explained using slightly simplified equations. Neglecting diffusion in the equation of turbulent energy balance, one can obtain the following solution of modified Equations (60), (61)

$$C^{-1/2} \equiv \tilde{u} = \frac{1}{k} \int_{\tilde{\zeta}_0}^{\tilde{\zeta}} \frac{(1 - \tilde{\tau})^{3/4}}{\tilde{\zeta}} \, d\tilde{\zeta}. \tag{65}$$

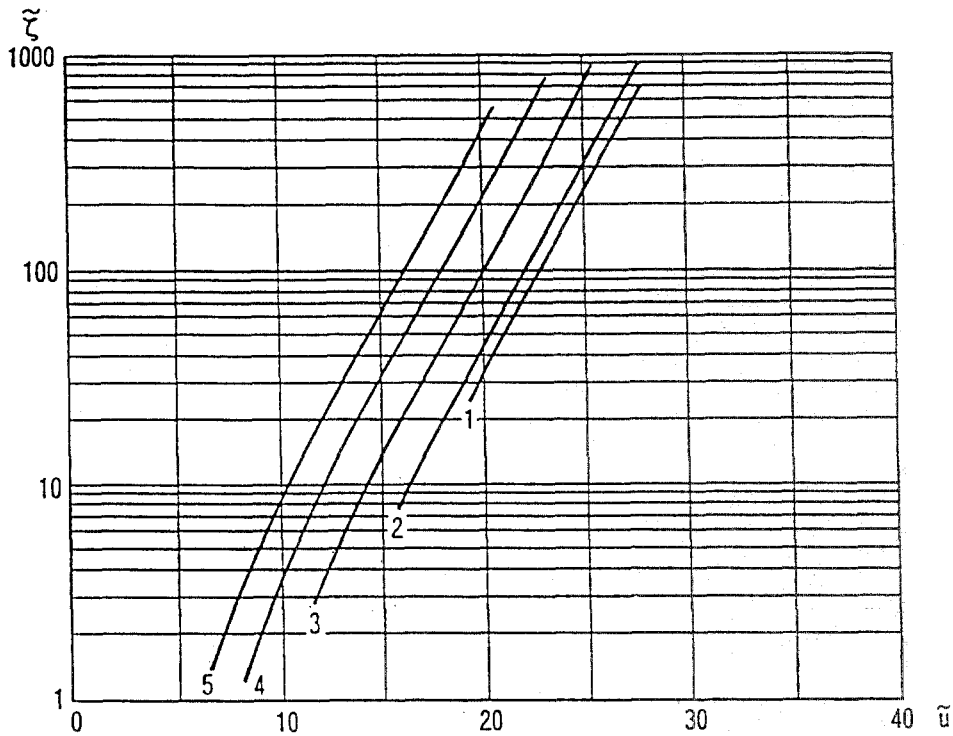

Fig. 6. Vertical profiles of wind velocity $|\tilde{\mathbf{u}}|$. Captions as in Figure 4.

Thus, the drag coefficient depends monotonically on the integral of the wave-induced momentum with respect to height.

Although $\tilde{\tau}$ at small heights may be sufficiently large, the wind profiles (Figure 6) reveal an insignificant departure from the logarithmic ones, but shift due to variations of the effective (total) roughness parameter. So, for any height except for a thin layer just near the surface, the following expression,

$$\tilde{z}_0 = \tilde{z}\, \mathrm{e}^{-k\tilde{u}} \tag{66}$$

gives in practice, the same values of the total roughness parameter.

The dependencies of $\tilde{z}_0$ and $\tilde{\zeta}_0$ on $\tilde{\omega}_p$ are shown in Figure 7. The values of $\tilde{\zeta}_0$ have been calculated using the formula

$$\tilde{\zeta}_0 = 0.075\, \tilde{\omega}_p^{3/4}, \tag{67}$$

which is derived from (54) and (55). It is easy to notice that $\tilde{z}_0$ varies with increasing $\tilde{\omega}_p$ to a greater extent than $\tilde{\zeta}_0$ does; this fact confirms the important role of wave-induced drag. The most convenient characteristic of the wave boundary layer is the drag law type:

$$C = f\left(\frac{u^2}{g\zeta}, \tilde{\omega}_p\right). \tag{68}$$

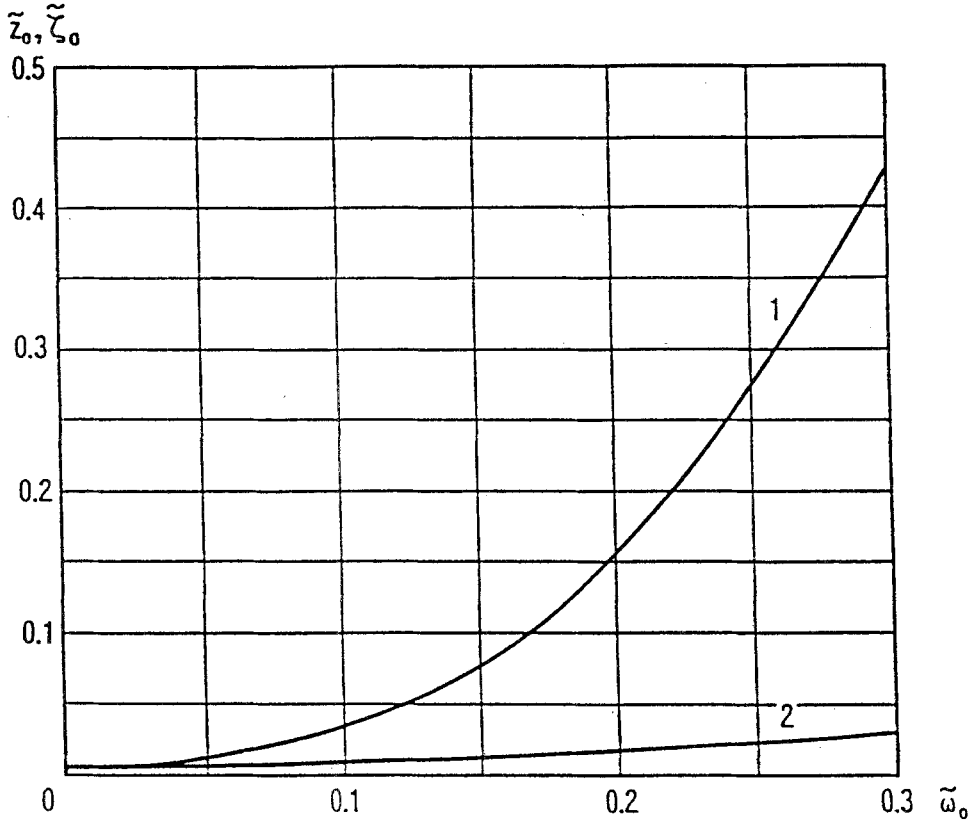

Fig. 7. Dependence of roughness parameters on peak frequency $\tilde{\omega}_p$: 1 – total roughness parameter $\tilde{z}_0$ (numerical solution), 2 – local roughness parameter $\tilde{\zeta}_0$ in accordance with (66).

This function, which was calculated by using the solution of Equations (60) and (61), is shown in Figure 8b. With increasing $u^2/g\zeta$ and $\tilde{\omega}_p$, the drag coefficient grows rather quickly. Relation (4), where the non-dimensional local roughness parameter $m = \zeta_0$ is calculated according to Equation (54), is shown in Figure 8a for comparison. This formula gives a weaker dependence of C on $\tilde{\omega}_p$ and $u^2/g\zeta$. Consequently, the drag over the sea surface is formed to a considerable extent by the specific wave situation but not the high-frequency universal part of the spectrum.

Using data in Figure 8, it is possible to derive the drag law which connects the drag coefficient at any arbitrary height ζ with external parameters $R = \ln(u^2/g\zeta)$ and $\Omega = \mathbf{u}/c_p$ (where u is the wind velocity at height ζ). This dependence may be approximated by the formula

$$\begin{aligned}\ln C = &-6.460 + 0.102\Omega + 0.009\Omega^2 \\ &+(0.311 + 0.055\Omega + 0.006\Omega^2)R \\ &+(0.032 + 0.011\Omega + 0.001\Omega^2)R^2. \end{aligned} \tag{69}$$

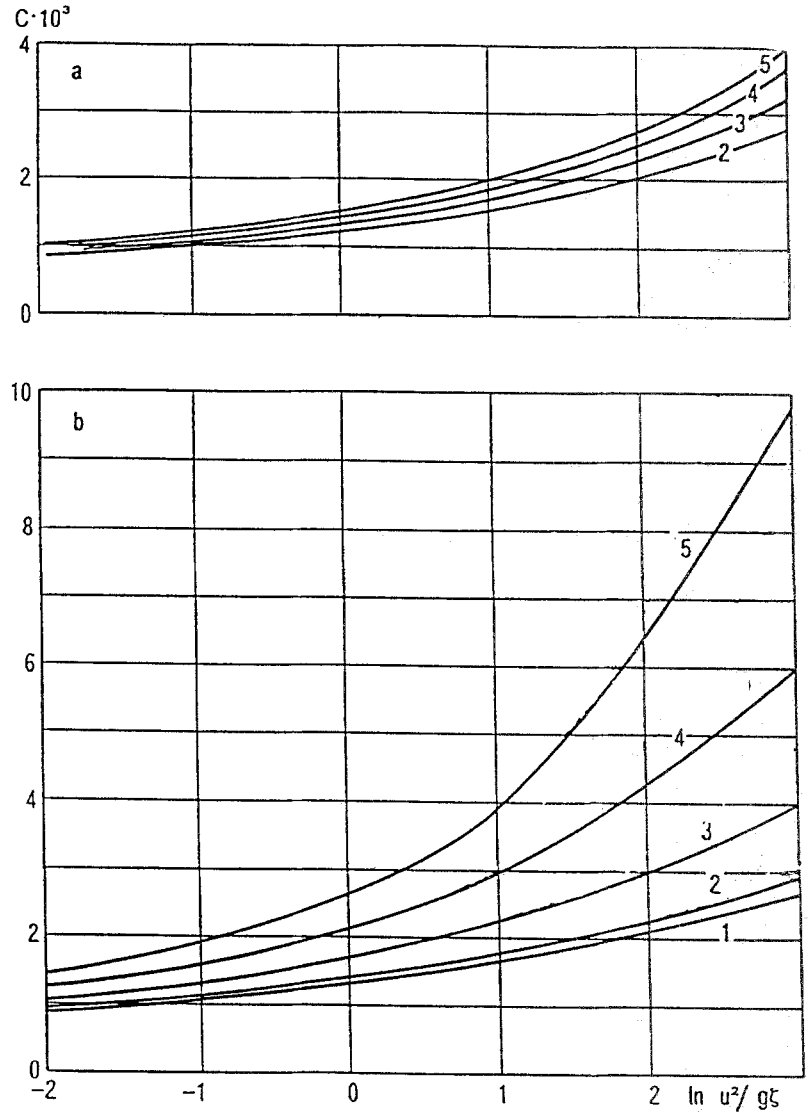

Fig. 8. Dependence of drag coefficient C at height z on $\ln(|\mathbf{u}|^2/gz)$, $\mathbf{u}$ – wind velocity at the same height: (a) $\tilde{\zeta}_0$ depends on $\tilde{\omega}_p$ only; (b) numerical solution. Captions as in Figure 4.

Unfortunately, reliable empirical data on the dependence of the drag coefficient or roughness parameter on fetch are scarce. To verify our theory, we used observations collected by Donelan (1982). They are displayed in Figure 9 together with the curves plotted according to Equation (69). Obviously, Figure 9 demonstrates qualitative agreement with experimental data.

The theoretical model uses the distance from the wave surface as a vertical coordinate. The point is that the wave drag mechanisms are formed close to the

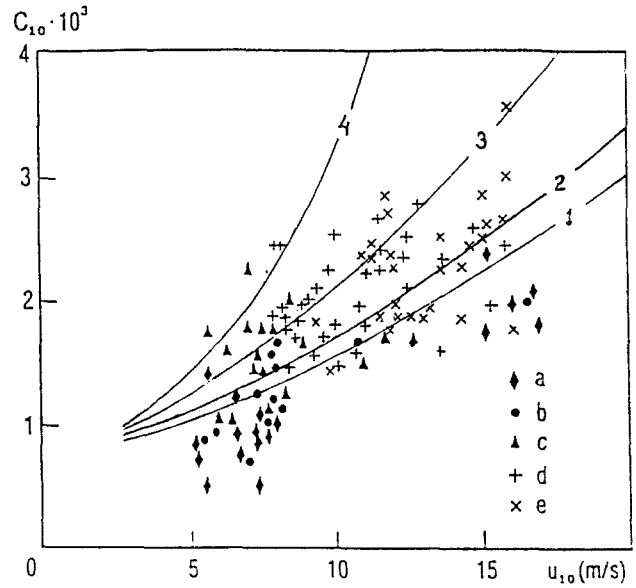

Fig. 9. Empirical dependence of the drag coefficient C_{10} on wind velocity u_{10} and $\tilde{\omega}_p$ (Donelan, 1982): a) $0.8 < \Omega < 1.5$; b) $1.5 < \Omega < 2.0$; c) $2.0 < \Omega < 3.0$; d) $3.0 < \Omega < 4.0$; e) $4.0 < \Omega < 6.0$. The curves represent the numerical solution: $1 - u_{10}/c_p = 0.8$; $2 - 1.15$; $3 - 2.5$; $4 - 3.5$.

surface and the use of the routine $\tilde{z}$-coordinate in 2-D or even 1-D models leads to a loss of the main physical properties in the wind-wave interaction process. Nevertheless, measurements are rarely performed in a following coordinate system. Therefore there is some reason to establish a relation between characteristics obtained by averaging at a fixed height $\tilde{z}$ and those at a fixed distance to the surface (Chalikov, 1978).

Any one-point moment $M(\tilde{z})$ in the $\tilde{z}$-coordinate system may be estimated using its vertical distribution $M(\tilde{\zeta})$ in the $\tilde{\zeta}$-coordinate as

$$M(\tilde{z}) = \int_{|\tilde{\eta}|<z} M(\tilde{z} - \tilde{\eta}) P(\tilde{\eta})\, \mathrm{d}\tilde{\eta}, \tag{70}$$

where $P(\tilde{\eta})$ is the probability distribution function

$$P(\tilde{\eta}) = \exp\left(- \frac{\tilde{\eta}^2}{\sigma^2} \right), \tag{71}$$

and σ is the root-mean-square deviation

$$\sigma^2 = 2 \int_0^\infty S(\tilde{\omega})\, \mathrm{d}\tilde{\omega}. \tag{72}$$

Vertical distributions of wind and wave momentum flux in the $\tilde{z}$- and $\tilde{\zeta}$-coordinates

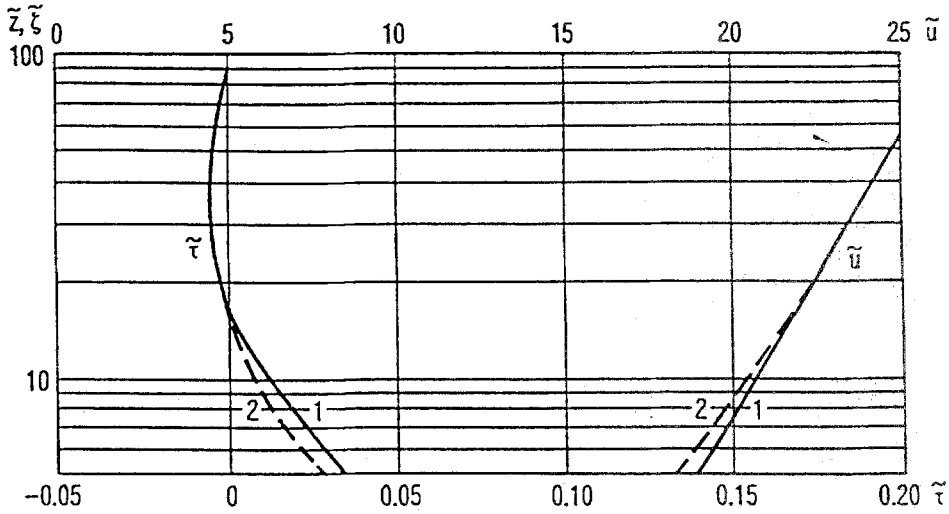

Fig. 10. The wind profile ($\tilde{u}$) and momentum flux profile ($\tilde{\tau}$) in $\tilde{z}$ (curves 1) and $\tilde{\zeta}$ (curves 2) coordinates.

for the Pierson–Moskovitz spectrum are shown in Figure 10 as an example. Both profiles above wave crests in the $\tilde{z}$-system are close to that in the $\tilde{\zeta}$-system. So the "following height" ζ in the definition of the external R-parameter may be replaced by the usual height z above mean water level.

6. Computation of Wave Boundary-Layer Structure, Energy and Momentum Fluxes to Waves and Currents for an Arbitrary Wave Field

This paper is devoted to a general investigation of the physical mechanisms responsible for drag above a wave surface. The main difference between the wave boundary layer and the boundary layer above an unmoving flat surface consists in the onset of an additional near-water momentum flux due to wave fluctuations of pressure, velocity and turbulent stress. Because the momentum balance takes place in a stationary boundary layer, the wave-produced momentum flux causes variations of turbulent momentum flux and deviations in the wind velocity profile from the logarithmic one inside and additive changes of wind velocity outside the wave boundary layer. Within the logarithmic interval of the wind profile, it is convenient to describe these effects by using the total roughness parameter which takes into account wave drag both in the low-frequency part of spectrum and in the universal range where Phillip's law is assumed.

The JONSWAP spectrum was used to illustrate these phenomena. However, the main objective of our work is an elaboration of a computational algorithm for the wave boundary-layer structure with an arbitrary wave field including waves produced by non-local wind. This problem has been formulated above (see Equations (40), (47) and boundary conditions (48), (57)). Let us reformulate this problem using dimensional variables for the case when the velocity at some height

h and 2-D wave spectrum $S(\omega, \theta)$, $(\omega < \omega_r)$ are known. For $\omega > \omega_r$, we suppose that the high-frequency part of spectrum is described by Phillips law $S = \alpha g^2 \omega^{-5}$ with given α. We shall use the z-coordinate system, but it is nesessary to keep in mind the effect demonstrated in Figure 8.

The structure of the stationary wave boundary layer is governed by the momentum balance equation

$$\frac{\partial}{\partial z}\left(K\frac{\partial u}{\partial z} + \tau\right) = 0, \tag{73}$$

where wave-induced momentum flux τ is equal to

$$\tau = \rho_w g \int_0^{\omega_r} \int_{\pi}^{\pi} \omega^2 \cos\theta S(\omega, \theta)\beta(\tilde{\omega}_a, C_\lambda)F(\xi. C_\lambda)\,\mathrm{d}\theta\,\mathrm{d}\omega. \tag{74}$$

Function β is defined by Equations (18), (19); function F, by Equation (35); K is the turbulent viscosity coefficient

$$K = l\sqrt{e}/c_1, \qquad l = kz. \tag{75}$$

Our computations showed that the diffusion term in the equation for turbulent energy usually is insignificant; so the equation for e can be taken in the form

$$\left(K\frac{\partial \mathbf{u}}{\partial z} + \frac{\tau}{\rho_a}\right)\cdot\frac{\partial \mathbf{u}}{\partial z} - \frac{K^3}{(kz)^4} = 0. \tag{76}$$

The term in the brackets describes the total vertical momentum flux which is equal to the turbulent stress $\mathbf{T}_h$ outside the wave boundary layer.

The lower boundary condition is

$$z = z_r: \quad K\frac{\partial \mathbf{u}}{\partial z} = \mathbf{T}_r = C_r|\mathbf{u}_r|\mathbf{u}_r. \tag{77}$$

In the general case, the wave spectrum is not symmetric with respect to the wind vector; hence, a lateral stress component may arise. In the joint ocean-atmosphere model, both components of $\mathbf{T}_h$ are to be taken into account in the following time step of the atmospheric model. The computed velocity profile may be used for computation of the energy flux to waves.

7. Discussion

Because the local thermodynamic interaction is a primary element of a multiscale ocean-atmosphere system, the accuracy of its parameterization predetermines the quality of weather forecasting and climate modeling to a considerable extent. Meanwhile, the existing approaches to parameterization of microscale interactions do not take into account many obvious mechanisms which can influence both media. In this paper, only the dynamical interaction is discussed. However, it is

7. Discussion

Because the local thermodynamic interaction is a primary element of a multiscale ocean-atmosphere system, the accuracy of its parameterization predetermines the quality of weather forecasting and climate modeling to a considerable extent. Meanwhile, the existing approaches to parameterization of microscale interactions do not take into account many obvious mechanisms which can influence both media. In this paper, only the dynamical interaction is discussed. However, it is possible to combine our 2–D equations with transfer equations for temperature and vapour and consider the density stratification effect.

The existing methods of momentum flux calculation are based on the Charnock relation, which does not take into account the specific character of a given wave field.

In all of the models, it assumed that the wind and wave fields are adapted to one another and that the wave spectrum is the spectrum of fully developed waves. Usually this is not correct because the space and time scales of a stationary wave field under a sufficiently strong wind are too large. Besides, waves produced by local wind are often superimposed on non-local swell. As a result, the drag coefficient depends on the 2–D wind-wave spectrum and wind velocity.

Surface waves play an important role in the dynamical regime of the ocean upper layer as well. In all of the mixed-layer models, waves are not taken into account and the whole momentum flux transfers to currents. In reality, a considerable part of this flux changes the wave momentum; it is redistributed over the spectrum due to non-linear interaction and goes back to the atmosphere through the inverse Miles mechanism, and to currents, by wave dissipation. This transition delay of momentum from wind to currents depends on the space and time scales of wave dissipation. Short waves give back their momentum almost locally whereas long waves carry it long distances. Besides, dissipation of wave energy intensifies turbulence in the mixed ocean layer.

Wind waves are an important regulator of dynamical interactions between the atmosphere and ocean. At present, there exist several spectral hydrodynamical models of wind waves. Probably, the most developed model is the WAM-model (WAMDI Group, 1988). This model is based on the equation

$$\frac{\partial S}{\partial t} + \mathbf{c}_g \cdot \nabla S = F_{nl} + F_{in} + F_{\text{diss}}, \tag{78}$$

which describes the transfer of wave energy density $S(\omega, \theta, t, x)$ by the group velocity $\mathbf{c}_g$, and its evolution due to non-linear interactions F_{nl}, wind input F_{in} and dissipation F_{diss}. Non-linear interactions are treated according to Hasselmann's theory (1962, 1963), somewhat simplified for computational reasons (Hasselmann and Hasselmann, 1985).

Energy input to waves is described by the F_{in} term in the form

$$F_{in} = \omega\beta(\omega, \theta)\, S(\omega, \theta), \tag{79}$$

where β is a wind-wave interaction parameter. Usually β is computed by using Snyder *et al.*'s (1981) relation which has been obtained experimentally from measurements of wave-induced pressure fluctuations. These measurements were carried out at a fixed height and then extrapolated to the wave surface using potential wave theory. Makin (1988) (see also Chalikov and Makin (1990)) showed that the decay parameter for pressure is very sensitive to non-dimensional wave frequency and deviates considerably from unity. In view of this, the method developed on the base of 2D models of the WBL (see Section 3 of the present paper) is preferable. Because the energy input depends on the wind profile, this method may be fully realized with joint boundary layer-wave models (see Section 6).

Dissipation of wave energy occurs mostly as a result of wave breaking, and the term F_{diss} is written by analogy with eq. (79)

$$F_{\text{diss}} = \omega\mathscr{D}(\omega, \theta) S(\omega, \theta), \tag{80}$$

where $\mathscr{D}(\omega, \theta)$ is a dissipative function (Komen *et al.*, 1984).

The general scheme of microscale dynamical interactions in a Wave Boundary Layer-Wind Waves-Mixed Layer system is shown in Figure 11a, b.

The wave spectrum in wave forecasting models is represented in a frequency range $(0, \omega_r)$. It is assumed that for $\omega > \omega_r$ the shape of the "subgrid" part of spectrum is universal. The frequency ω_r predetermines the lowest level of the numerical model $\zeta_r \simeq g/\omega_r^2$ where the local quadratic law Equation (77) is introduced.

The momentum flux from wind to waves is equal to

$$\tau_0 = \rho_w g \int_0^{\omega_r} \int_{\pi}^{\pi} \mathbf{k} S(\omega m, \theta) \beta(\omega, \theta)\, \mathrm{d}\theta\, \mathrm{d}\omega, \tag{81}$$

and the momentum transferred from waves to the currents due to dissipation is equal to

$$\tau_c = \rho_w g \int_0^{\omega_r} \int_{\pi}^{\pi} \mathbf{k} S(\omega, \theta) \mathscr{D}(\omega, \theta)\, \mathrm{d}\theta\, \mathrm{d}\omega. \tag{82}$$

The momentum flux from wind to waves in the "subgrid tail" of the spectrum,

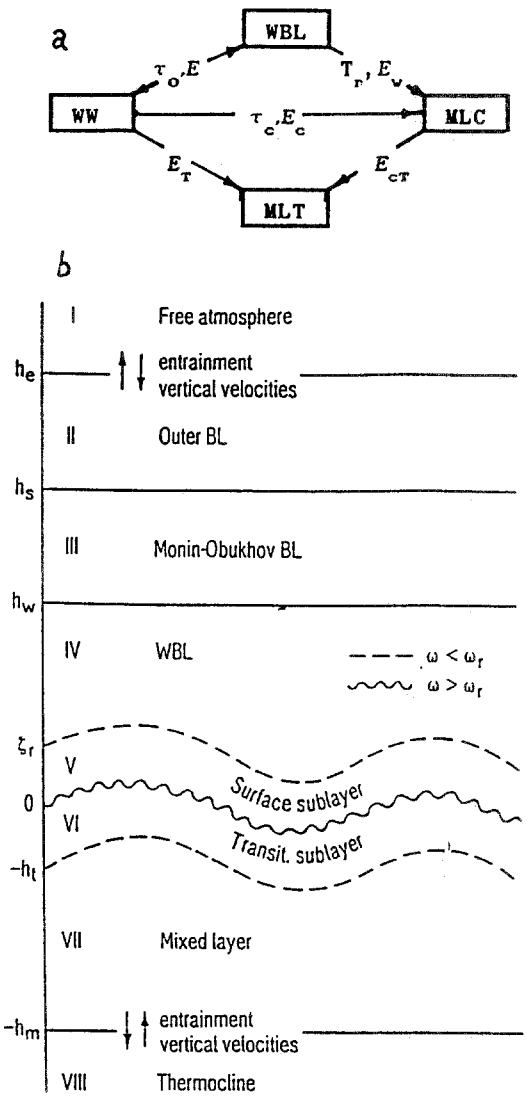

Fig. 11. (a) Scheme for energy and momentum exchange between Wave Boundary layer (WBL), Wind Waves (WW), Mixed layer currents (MLC) and Mixed Layer Turbulence (MLT). τ_0 – momentum exchange between WBL and WW (81); τ_c – between WW and MLC (82); T_r – between WBL and MLC (77). E – energy exchange between WBL and WW (83), E_c – between WW and MLC (86); E_{cT} – between MLC and MLT. (b) General scheme of the ocean-atmosphere interacting system (for explanation, see text).

which immediately transfers to the current, is given by Equation (77). The total momentun flux to the current $\tau_c + \mathbf{T}_r$ provides the upper boundary condition for computation of wind- and wave-driven currents. Total energy exchange between wind and waves is given by

$$E = \rho_w g \int_0^{\omega_r} \int_{\pi}^{\pi} \omega S(\omega, \theta) \beta(\omega, \theta) \, \mathrm{d}\theta \, \mathrm{d}\omega. \tag{83}$$

The energy flux from waves to currents is equal to

$$E_c = \tau_c \cdot \mathbf{u}_c \tag{84}$$

($\mathbf{u}_c$ is the surface current velocity); and from wind to currents

$$E_w = \mathbf{T}_r \cdot \mathbf{u}_c. \tag{85}$$

Dissipating waves also produce a turbulent energy flux E_T to the ocean upper layer, which is used as the boundary condition in the mixed-layer model.

$$E_T = \rho_w \mathbf{g} \int_0^{\omega_r} \omega S(\omega, \theta) \mathscr{D}(\omega, \theta) \, \mathrm{d}\theta \, \mathrm{d}\omega - E_c. \tag{86}$$

Production of turbulent energy E_{cT} due to turbulent dissipation of orbital wave velocities can be easily considered as well.

The wave boundary layer includes regions *IV*, *V* of Fig. 11b. In region *III* for neutral stratification the wind profile is a logarithmic one with total roughness parameter produced by wave and local drag (formula (69)). In region *IV*, where the upper bound lies at height h_w of order $0.1\lambda_p$ (λ_p is wavelength at the spectral peak), a wave-induced flux of momentum arises, produced by waves with spectrum $S(\omega, \theta)$, $0 < \omega < \omega_r$. The higher frequencies are taken into account in sublayer *V* where subgrid waves form the local roughness parameter (54) and tangential stress Eq. (77). Because the height of the wave boundary layer h_w is usually much smaller than the Monin–Obukhov length scale L, stratification is close to neutral; and the effects of stratification may be taken into account in region *III*. Above it lies the outer part of the boundary layer where it is necessary to introduce the Coriolis force.

The non-homogeneity of the stress field over the ocean surface due to the variable wave field amplifies the vertical motions at upper levels of the planetary layer. So, it is quite possible that wind waves affect weather and climate.

The mixed layer VII obtains its momentum and turbulent energy via transition zone *VI* (formulae (81), (83)).

In this paper, we have presented a theory of the boundary layer above a wave surface with an arbitrary spectrum. It uses the results of a 2–D numerical simulation of the boundary layer above monochromatic waves, namely, a vertical profile of wave-induced momentum flux and a parameter of wind-wave interaction in broad ranges of wave frequencies and values of the drag coefficient. We supposed that the superposition principle is appropriate for a multimode surface. It is important that the wind-wave interaction parameter is negative for waves with apparent phase velocity greater than wind speed. Probably, this effect provides stabilization of the wind-wave spectrum at constant wind.

Equations describing the structure of the wave boundary layer are derived.

Concepts of local and total roughness parameters and drag coefficients are considered. It is supposed that at heights where the drag is formed by high-frequency waves with spectrum $S\omega^{-5}$, the local roughness parameter depends on Phillips' constant α only. This dependence has a weak influence on the total drag coefficient whose variability is mainly under the influence of the wave momentum fluxes produced by lower-frequency waves.

The model is used to simulate the 1-D structure of the wave boundary layer with the wave field described by the JONSWAP spectrum. It is shown that with decreasing fetch, the total energy input increases whereas the momentum flux decreases. This is explained by the overshoot effect and energy growth in the high-frequency part of the spectrum with decreasing fetch.

The wind velocity profile in all cases is close to the logarithmic profile. So inside the boundary layer (except for its lowest part) it is sufficient to know the total roughness parameter which grows rather quickly with decrease in fetch. Near the surface in the following coordinate system, the wind profile deviates from the logarithmic one due to the wave-induced momentum flux which weakens the turbulent stress.

A drag law for developing waves is suggested. It describes the above-mentioned effects with sufficient accuracy.

A 1-D model of the wave boundary layer above an arbitrary wave field has been elaborated. This model allows calculations of spectral distributions of energy and momentum exchange as well as the turbulent stress vector at the upper bound of the wave boundary layer. This kind of model must be an essential part of any atmosphere – wind waves – ocean joint model.

The main mechanisms responsible for the surface wave influence on the ocean – atmosphere system are enumerated.

Acknowledgements

We should like to thank Dr. V. K. Makin who provided us with data concerning the vertical distribution of the momentum flux and wind-wave interaction parameter; and Dr. Y. Toba and Dr. K. Marine for valuable comments on the manuscript. This work was completed in the National Meteorological Center (U.S.A). The authors wish to extend their thanks to Dr. E. Kalnay and Dr. D. Rodenhuis for their encouragement.

References

Benilov, A., Gumbatov, A., Zaslavsky, M., and Kitaigorodskii, S. A.: 1978, 'Non-Steady Model of Development of Turbulent Boundary Layer Above Sea Under Generating of Surface Waves', *Izv. Acad. Sci. of the USSR Atmos. Ocean Phys.* **14**, 1177.

Burgers, G. and Makin V.: 1991, 'Boundary Layer Model Results for Wind-Sea Growth', *J. Phys. Oceanogr.* (in press).

Chalikov, D.: 1976, 'A Mathematical Model of Wind-Induced Waves', *Dokl. Akad. Nauk SSSR* **229**, 1083.

Chalikov, D.: 1978, 'The Numerical Simulation of Wind-Wave Interaction', *J. Fluid Mech.* **87**, 561–582.

Chalikov, D.: 1980, *Mathematical Modelling of Wind-Induced Waves. News and Problem of Science*, Gidrometeoizdat, Leningrad, p. 48.

Chalikov, D.: 1986, 'Numerical Simulation of the Boundary Layer Above Waves', *Boundary-Layer Meteorol.* **34**, 63–98.

Chalikov, D.: 1992, 'Comments on "Wave Induced Stress and the Drag of Air Flow over Sea Waves" and "Quasi-linear Theory of Wind-Wave Generation Applied to Wave Forecasting"', (accepted in *Journ. Phys. Oceanogr*).

Chalikov, D. and Makin, V.: 1990, 'Pressure Distribution Above Waves', EGS, XV General Assembly Copenhagen, 23–27 April 1990, *Ann. Geophysicae*, spec. iss., 198.

Chalikov, D. and Makin, V.: 1991, 'Models of the Wave Boundary Layer', *Boundary-Layer Meteorol.* **56**, 83–99.

Charnock, H.: 1955, 'Wind Stress on a Water Surface', *Quart. J. Roy. Meteorol. Soc.* **81**, 639.

Donelan, M. A.: 1982, 'The Dependence of the Aerodynamic Drag Coefficient on Wave Parameters',. in *Proc. First Int. Conf. on Meteor. and Air-Sea Interaction of the Coastal Zone*, The Hague, Amer. Meteorol. Soc., p. 381.

Garratt, J. R.: 1977, 'Review of Drag Coefficient Over Oceans and Continent', *Mon. Wea. Rev.* **105**, 915.

Hasselmann, K., 1962, 'On the Non-Linear Energy Transfer in a Gravity-Wave Spectrum. 1. General Theory'. *J. Flud Mech.* **12**, 481.

Hasselmann, K.: 1963, 'On the Non-Linear Energy Transfer in a Gravity-Wave Spectrum. 2. Conservation Theorems, Wave-Particle Correspondence, Irreversibility', *J. Fluid Mech.* **15**, 273.

Hasselmann, K., Barnett, T. P., Bouws, E., Carlson H., Cartwright, D. E., Enke, K., Ewing, J. A., Gienapp, H., Hasselmann, D. E., Kruseman, P., Meerburg, A., Muller, P., Olbers, D. J., Richter, K., Sell, W. and Walden, H.: 1973, 'Measurements of Wind-Wave Growth and Swell Decay During the Joint Sea Wave Project (JONSWAP), *Dtsch. Hydr. Z.* **A8**(12), 1.

Hasselmann, D. E., Dunckel, M. and Ewing, J. A.: 1980, 'Directional Wave Spectra Observed During JONSWAP 1973', *J. Phys. Oceanogr.* **10**, 1264.

Hasselmann, S. and Hasselmann, K.: 1985, 'Computations and Parameterization of the Non-Linear Energy Transfer in a Gravity-Wave Spectrum', Part 1: A New Method for Efficient Computations of the Exact Non-Linear Transfer Integral', *J. Phys. Oceanogr.* **15**, 1369.

Hsiao, S. V. and Shemdin, O. H.: 1983, 'Measurements of Wind Velocity and Pressure with a Wave Follower During MARSEN', *J. Geophys. Res.* **88**(C14), 9841.

Janssen, P. A. E. M.: 1989, 'Wind-Induced Stress and the Drag of Air Flow Over Sea Waves', *J. Phys. oceanogr.* **19**, 745.

Janssen, P. A. E. M.: 1991, 'Quasi-linear Theory of Wind-Wave Generation Applied to Wave Forecasting', *J. Phys Oceanogr.* **21**, 1631–1642.

Komen, G. J., Hasselmann, S. and Hasselmann, K.: 1984, 'On the Existence of a Fully Developed Wind-Sea Spectrum', *J. Phys. Oceanogr.* **14**, 1271.

Makin, V.: 1987, 'Numerical Results on the Structure of the Sea Wave-Induced Pressure Field in Atmosphere', *Morsoy Gidrofizicheskiy Zhurnal* No. 2, 50.

Makin, V.: 1989, 'The Dynamics and Structure of the Boundary Layer Above Sea', Senior doctorate thesis. Inst. of Oceanology, Acad. of Sci. of the USSR, Moscow, p. 417 (in Russian).

Makin, V. and Chalikov, D.: 1986, 'The Spectral Structure of Boundary Layer Above Sea Waves', *Sov. Phys. Doklady* **287**, No. 3.

Makin, V. and Chalikov, D.: 1986, 'Calculating Momentum and Energy Fluxes Going to Developing Waves', *Izv. Atmos. Ocean. Phys.* **22**, 1015–1019.

Panchenko E. and Chalikov, D.: 1984, 'Energy Structure of the Surface Layer Above the Sea Waves', *Izv. Atmos. Ocean. Phys.* No. 2, 732–737.

Plant W. J.: 1982, 'A Relationship Between Wind Stress and Wave Slope', *J. Geophys. Res.* **87**(C3), 1961–1967.

Smith, S. D. and Banke, E. G.: 1975, 'Variation of the Sea Surface Drag Coefficient with Wind Speed', *Quart. J. Roy. Meteorol. Soc.* **101**, 665.

Snyder, R. L., Dobson, F. W., Elliot, J. A. and Long, R. B.: 1981, 'Array Measurements of Atmospheric Pressure Fluctuations Above Gravity Waves', *J. Fluid Mech.* **102**, 1.

Toba, Y., Iida, N., Kawamura, H., Ebuchi, N., and Jones, I. S. F.: 1990, 'Wave Dependence of Sea-Surface Wind Stress', *J. Phys. Oceanogr.* **20**, 705.

Van Duin, C. A. and Janssen, P. A. E. M.: 1992, 'An Analytic Model of the Generation of Surface Gravity Waves by Turbulent Air Flow', *J. Fluid Mech.* **236**, 197–215.

WAMDI Group (Hasselmann, S., Hasselmann, K., Banner, E., Janssen, P. A. E. M., Komen, G. J., Bertotti, L., Lionello, P., Guillaume, A., Cardone, V. J., Greenwood, J. A., Reistad, M., Zambresky, L. and Ewing, J. A.): 1988, 'The WAM Model – A Third Generation Ocean Wave Prediction Model', *J. Phys. Oceanogr.* **18**, 1775.

Wu, J.: 1980, 'Wind-Stress Coefficient Over Sea Surface Near Neutral Conditions – a Revisit', *J. Phys. Oceanogr.* **10**, 727.